Review Article

Imaging of pulmonary hypertension: an update

Harold Goerne[1,2], Kiran Batra[3], Prabhakar Rajiah[3]

[1]IMSS Centro Medico Nacional De Occidente, Guadalajara, Jalisco, Mexico; [2]CID Imaging and Diagnostic Center, Guadalajara, Jalisco, Mexico; [3]Radiology Department, UT Southwestern Medical Center, Dallas, Texas, USA

Contributions: (I) Conception and design: H Goerne, P Rajiah; (II) Administrative support: H Goerne, P Rajiah; (III) Provision of study materials or patients: All authors; (IV) Collection and assembly of data: H Goerne, P Rajiah; (V) Data analysis and interpretation: H Goerne, P Rajiah; (VI) Manuscript writing: All authors; (VII) Final approval of manuscript: All authors.

Correspondence to: Prabhakar Rajiah, MD. Associate Professor, Department of Radiology, Cardiothoracic Imaging, UT Southwestern Medical Center, E6.120 B, Mail code 9316, 5323 Harry Hines Boulevard, Dallas, TX 75390-8896, USA. Email: radprabhakar@gmail.com.

Abstract: Pulmonary hypertension (PH) is characterized by elevated pulmonary arterial pressure caused by a broad spectrum of congenital and acquired disease processes, which are currently divided into five groups based on the 2013 WHO classification. Imaging plays an important role in the evaluation and management of PH, including diagnosis, establishing etiology, quantification, prognostication and assessment of response to therapy. Multiple imaging modalities are available, including radiographs, computed tomography (CT), magnetic resonance imaging (MRI), nuclear medicine, echocardiography and invasive catheter angiography (ICA), each with their own advantages and disadvantages. In this article, we review the comprehensive role of imaging in the evaluation of PH.

Keywords: Computed tomography (CT); pulmonary; hypertension; dual-energy; magnetic resonance imaging (MRI); nuclear

Submitted Dec 12, 2017. Accepted for publication Jan 08, 2018.
doi: 10.21037/cdt.2018.01.10
View this article at: http://dx.doi.org/10.21037/cdt.2018.01.10

Introduction

Pulmonary hypertension (PH) is a progressive disorder characterized by elevated pulmonary arterial pressure. It is caused by a multitude of intrinsic and extrinsic pulmonary vascular disease processes that cause hemodynamic alterations which overcome the normal pulmonary vasoregulatory mechanisms. PH is an important cause of mortality and morbidity, accounting for approximately 200,000 hospitalizations and 15,000 deaths per year in the USA (1), with an estimated prevalence of 10 to 52 cases per million (2). Multiple imaging modalities are available, including radiograph, echocardiography, nuclear medicine, invasive catheter angiography (ICA), computed tomography (CT) and magnetic resonance imaging (MRI), each with their own advantages and disadvantages.

In this article, we review the comprehensive role of imaging in the evaluation of PH.

Classification, pathophysiology and clinical features

PH is diagnosed when the mean pulmonary artery pressure (mPAP) is ≥25 mmHg at rest in right heart catheterization (RHC) (3). PH was earlier classified as primary and secondary types or precapillary and post-capillary types. Precapillary type has low pulmonary capillary wedge pressure (PCWP) of <15 mmHg, while the post-capillary type has high PCWP >15 mmHg. In 2013, the World Health Organization (WHO) classified PH into five types based on the etiology (*Table 1*) (4). Group 1 includes diseases centered in the small arterioles [pulmonary arterial hypertension (PAH)]. These are predominantly precapillary types, although pulmonary veno-occlusive disease (PVOD) and pulmonary capillary hemangiomatosis (PCH), which are post-capillary types are also included in this group due to similar clinical presentation (5). PAH is diagnosed when

Table 1 Causes of pulmonary hypertension (based on Updated classification of pulmonary hypertension from 5th WSPH Nice 2013) (4)

No	Type	Entities
1	Pulmonary arterial hypertension	1.1 Idiopathic PAH
		1.2 Heritable PAH (BMPR2, ALK-1, ENG, SMAD9, CAV1, KCNK3, unknown)
		1.3 Drug and toxin induced
		1.4 Associations with other diseases (connective tissue disease, HIV, portal hypertension, congenital heart disease, schistosomiasis)
		1' Pulmonary veno-occlusive disease and/or pulmonary capillary hemangiomatosis
		1" Persistent pulmonary hypertension of the newborn (PPHN)
2	Left heart disease	2.1 Left ventricular systolic dysfunction
		2.2 Left ventricular diastolic dysfunction
		2.3 Valvular disease
		2.4 Congenital/acquired left heart inflow/outflow tract obstruction and congenital cardiomyopathies
3	Lung diseases and/or hypoxia	3.1 Chronic obstructive pulmonary disease
		3.2 Interstitial lung disease
		3.3 Other pulmonary diseases with mixed restrictive and obstructive pattern
		3.4 Sleep-disordered breathing
		3.5 Alveolar hypoventilation disorders
		3.6 Chronic exposure to high altitude
		3.7 Developmental lung diseases
4	Chronic thromboembolic pulmonary hypertension (CTEPH)	–
5	Unclear multifactorial mechanisms	5.1 Hematologic disorders (chronic hemolytic anemia, myeloproliferative disorders, splenectomy)
		5.2 Systemic disorders (sarcoidosis, pulmonary histiocytosis, lymphangioleiomyomatosis)
		5.3 Metabolic disorders (glycogen storage disease, Gaucher disease, thyroid disorders)
		5.4 Others (tumoral obstruction, fibrosing mediastinitis, chronic renal failure, segmental PH)

PAH, pulmonary arterial hypertension; PH, pulmonary hypertension.

there is high PAP, high PVR (>3 Woods units) and low PCWP (<15 mmHg), but without evidence of other precapillary types of PH. Group 2 is the most common type in USA (6) and includes disorders of the left heart, including valvular and outflow tract obstructive lesions. PH is observed in 60–70% of patients with LV dysfunction, either systolic or diastolic (7). PCWP is elevated in these patients with obstruction at the post-capillary level. Group 3 includes disorders of the lung and other hypoxic diseases with associated vasoconstriction. PCWP is normal in these patients and it is unusual to have severe PH in this group except in the case of combined pulmonary fibrosis and emphysema (5). Group 4 is caused by chronic thromboembolic pulmonary hypertension (CTEPH) and other diseases of pulmonary artery obstruction such as neoplasms, congenital pulmonary artery stenosis, arteritis, and hydatid cyst (6). Group 5 involves miscellaneous entities with unclear and multi-factorial mechanisms.

There are three clinical phases of PH, namely the asymptomatic compensated, symptomatic compensated and advanced decompensated phases (7-9). Clinical symptoms are often variable and include dyspnea, fatigue, syncope, chest pain and Raynaud phenomenon. Symptoms of right heart failure are seen in the late

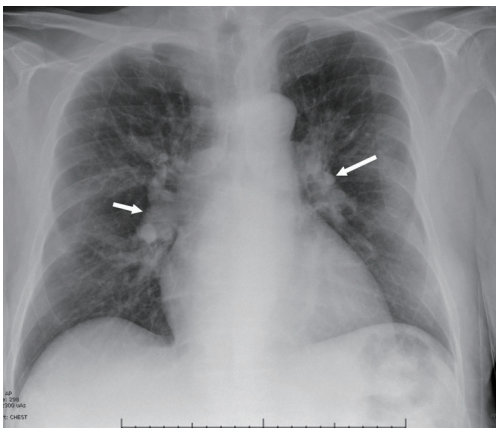

Figure 1 Chest radiograph. Posteroanterior (PA) chest radiograph shows dilated central pulmonary arteries (arrows), consistent with pulmonary arterial hypertension.

stages, eventually resulting in death if untreated. Since the symptoms are non-specific, high level of suspicion of PH should be present in patients with connective tissue diseases, pulmonary thromboembolism and congenital heart disease (CHD) (9). Other symptoms are present depending on the underlying cause, such as symptoms of heart failure in group 2 and lung disorders in group 3 and recurrent DVT in group 4. Physical signs include hypotension, tachycardia, low oxygen saturation, elevated JVP with 'a' wave, loud P2, cardiac murmurs, hepatomegaly, ascites and edema. BNP, pro-BNP and high-sensitive troponin may be elevated and uric acid level is low (6). Six-minute walk test, ABG and PFT are also performed for functional evaluation. ECG shows right axis deviation in RVH, along with high R waves in right leads, S1Q3T3 pattern and features of left/right heart disease. Frequent premature atrial contraction, atrial tachycardia or atrial fibrillation may also be seen (6).

Imaging techniques in the evaluation of PH

The main role of imaging is to establish the diagnosis of PH and classify the PH into one of the five groups. Imaging is also used in the quantification of volumes and function, which is essential for prognosis, therapy, and assessing response to treatment.

Chest radiograph

Chest radiograph is a commonly used imaging modality in the evaluation of PH. The classic radiographic pattern of PH is enlargement of central pulmonary arteries (i.e., right interlobar pulmonary artery >15 mm in women or >16 mm in men), with or without pruning of the peripheral arteries (*Figure 1*). RV dilatation is seen in advanced stages (10), with enlargement of the cardiac silhouette in PA radiograph and obliteration of the retrosternal clear space in the lateral radiograph. Right heart border appears prominent due to right atrial enlargement. Chest radiograph has been shown to have high sensitivity (97%) and specificity (99%) in the detection of PH (11,12), but a normal chest radiograph does not exclude PH, especially in patients with mild disease. Chest radiograph is also useful in the diagnosis of causes of PH such as emphysema, ILD, chest wall deformities, and left-heart disease. In CTEPH, areas of oligemia, pleural thickening and scarring may be seen.

Echocardiography

Transthoracic echocardiography (TTE) is an essential tool in the evaluation of patients with suspected PH. It is widely available, portable, non-invasive, inexpensive and has no radiation. Echocardiography has good spatial and high spatial resolution, that provides morphological, functional and hemodynamic analysis. Limitations include operator dependence and limited field-of-view, especially in patients with obesity, emphysema or chest wall deformities. TTE is often the initial screening modality used in the diagnosis of PH, particularly in patients with gene mutations, first-degree relative with PH, congenital disease, connective tissue disease or portal hypertension. Pulmonary artery systolic pressure (PASP) can be estimated using the equation $4\times (\text{V-TR})^2 + \text{RAP}$, where V-TR is the peak velocity of the tricuspid regurgitant jet and RAP is the right atrial pressure which is estimated based on the size of IVC and its respiratory variation (13) (*Figure 2A*). mPAP can also be estimated using the formula, $4\times (\text{V-PR})^2 + \text{RAP}$, where V-PR is the peak pulmonary regurgitant velocity, which is estimated from the formula $\text{VTR}/\text{TVI}_{\text{RVOT}} \times 10+0.16$, where TVI_{RVOT} is time velocity integral of right ventricular outflow tract (14). Based on the TTE values, the patient can be placed in low, intermediate or high probability of PH. An estimated systolic pulmonary pressure >50 mmHg justifies invasive evaluation in symptomatic patients (7). Echocardiography is not sensitive in mild and asymptomatic PH.

Other features of PH include—RV dilation (*Figure 2B*); RVOT dilation; RV hypertrophy; RV dysfunction; RA dilation; elevated RA pressure; abnormal septal bowing

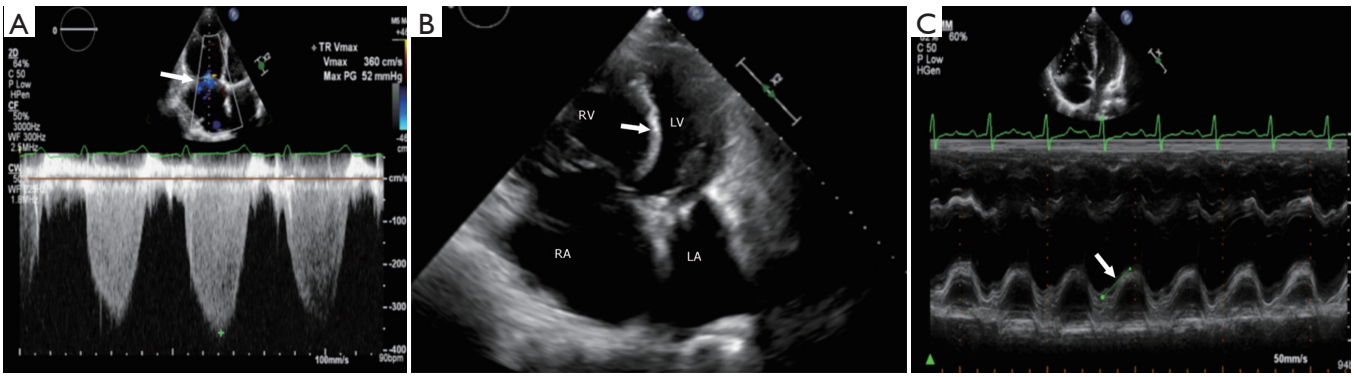

Figure 2 Echocardiography. (A) Doppler echocardiogram showing measurement of the velocity of the tricuspid regurgitation jet (arrow), which is used to estimate the systolic pulmonary arterial pressure. (B) Four-chamber echocardiogram showing dilation of the right ventricle (RV) and bowing of the ventricular septum (arrow) to the left. (C) Measurement of tricuspid annular plane systolic excursion (TAPSE) using M-mode echocardiogram (arrow). RA, right atrium; LV, left ventricle; LA, left atrium.

with D-shaped LV (*Figure 2B*); dilated pulmonary artery; abnormal blood flow velocity and pattern out of RV; atrial septal bowing; mid-systolic notch pattern; and pericardial effusion (6). 3D echocardiogram is promising for quantification of volumes and function, including of RV; however more studies and experience are required to validate this modality (15). Since evaluation of the RV is challenging with echocardiography due to its complex shape and limited acoustic window, RV function can be indirectly estimated using tricuspid annular plane systolic excursion (TAPSE) (*Figure 2C*). Tei myocardial performance index (MPI) is (isovolumic contraction + iso-relaxation time)/ ejection time), with low values indicating effective ejection of blood from RV (16). Tei MPI >0.83 was shown to have poor 5-year survival of <10% in patients with idiopathic PH (17). With speckle tracking, low peak RV longitudinal strain in PH correlates with higher mortality and worsening functional status (18). Echocardiography can also be used to evaluate cardiac anatomy, but provides only limited information on extra-cardiac structures. It is useful in evaluating the group 2 causes of PH. Bubble studies can be used for evaluating cardiac shunts. Transesophageal echocardiogram (TEE) has some role in the evaluation of complex cardiac shunts, but this can be easily assessed non-invasively with CT or MRI.

Nuclear medicine

Radionuclide V/Q scanning is commonly used in the diagnosis of CTEPH in all patients with unexplained PH (11). It has a high sensitivity of 90–100% and specificity of 94–100% in distinguishing CTEPH from idiopathic PAH (IPAH) (7,13). Although some earlier studies showed that V/Q scan was more sensitive than CTPA in detecting CTEPH (Sensitivity 97% *vs.* 51%, specificity 95% *vs.* 99%) (19), recent studies show that CTPA has comparable sensitivity and specificity (20). CTEPH is diagnosed when there is a ≥1 segmental or larger mismatched perfusion defect with normal ventilation (*Figure 3*). This can be distinguished from IPAH and PVOD, which have normal perfusion or sub-segmental mottled defects (5). Low probability or normal V/Q scan excludes CTEPH as a diagnosis with sensitivities and specificities up to 100% (11). The assessment of lung parenchymal perfusion also serves as a reasonable parameter for estimating postoperative PVR in patients with CTEPH undergoing pulmonary thromboendarterectomy (PEA). However, there are several limitations of the modality, including a high number of non-diagnostic and non-specific studies as well as lack of anatomical information (21). Mismatched defects may also be seen rarely in PVOD and PCH (21). False positive mismatched defects can also be seen in vasculitis, fibrosing mediastinitis, radiation-fibrosis and neoplasms of pulmonary artery (5). Occasionally CTEPH may produce matched defects due to reduced ventilation from chronic hypoperfusion (5). V/Q scan also underestimates the degree of vascular obstruction and hemodynamic abnormalities in CTEPH, likely due to the presence of thrombus recanalization and collateral vessel formation, which may deliver the isotopes even to the periphery of the lungs (5).

SPECT/CT can be utilized to improve the performance of V/Q scan. The non-contrast CT is useful not only for

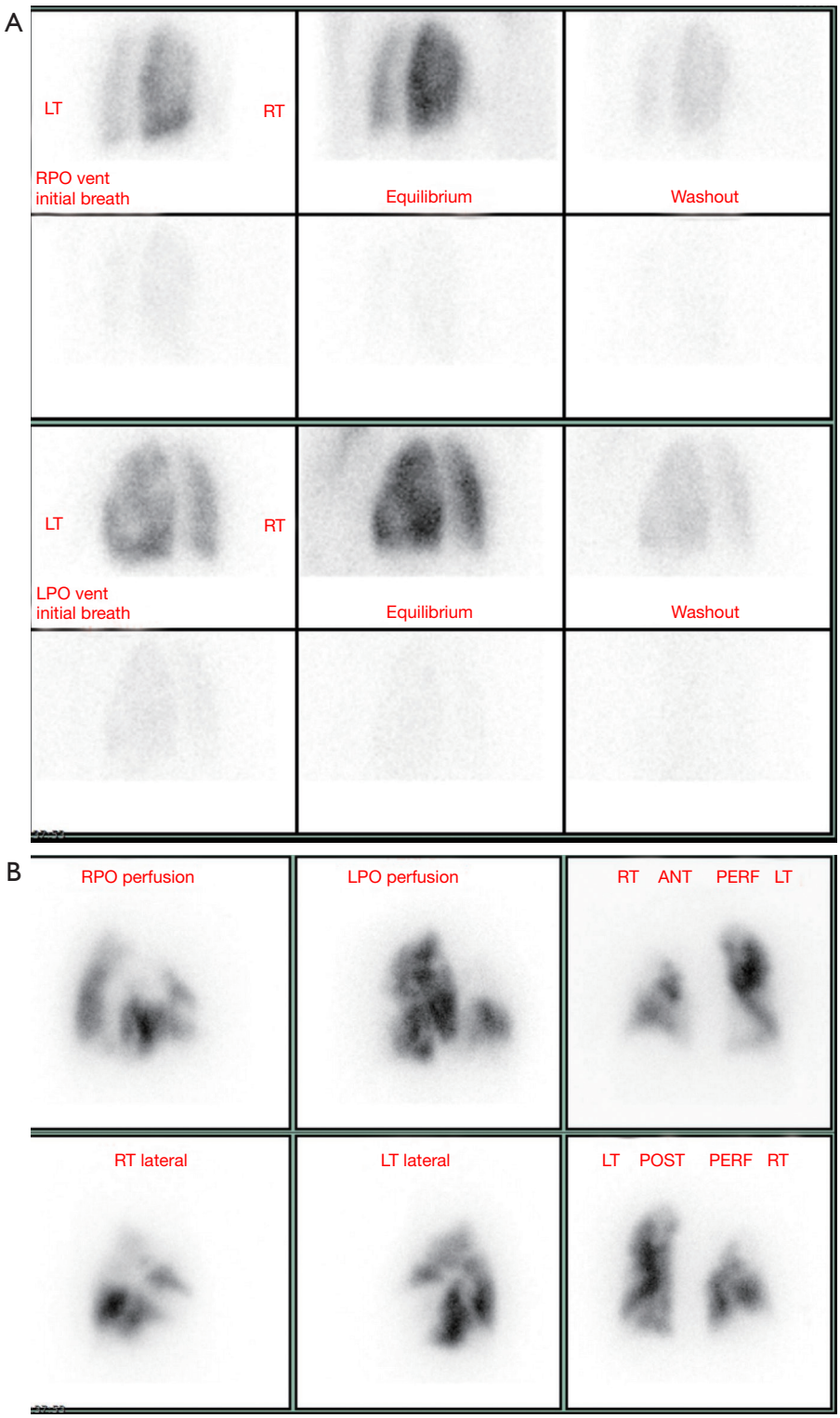

Figure 3 V/Q scan. (A) Ventilation scan in a patient with pulmonary hypertension shows normal ventilation in the right lung and slightly decreased ventilation in central area of left lower lobe. (B) Perfusion scan in the same patient shows heterogeneous perfusion with multiple mismatched perfusion defects bilaterally. This is a high probability scan for chronic thromboembolic pulmonary hypertension. LT, left; RT, right; LPO, left posterior oblique; RPO, right posterior oblique.

Figure 4 Pulmonary angiography. Frontal pulmonary angiographic image in a patient with pulmonary hypertension shows multifocal areas of stenosis and post-stenotic dilation, involving lobar, segmental and sub-segmental arteries (arrows).

attenuation correction, but also to exclude non-embolic causes of perfusion defects. This technique is more sensitive in identifying obstructed segments and can evaluate regional functional information and pulmonary vascular reserve from 3D fusion images and may be used to assess pulmonary vascular reserve (22,23). There is limited role of 18F-FDG PET in the evaluation of PH, particularly in distinguishing pulmonary sarcoma from a CTEPH, with the former showing high uptake. High uptake is also seen in rare entities such as Takayasu arteritis (11). In patients with IPAH, high FDG uptake has been shown in the RV myocardium as well as the lungs (11). Poor prognosis has been demonstrated in PH patients with SUV >8.3 in RV free wall (24).

Invasive catheter angiography

ICA is the current gold standard in the diagnosis of PH, since it is the only technique that directly and accurately determines PAP. RHC is used for diagnosing PH in patients with intermediate or high probability in echocardiography, indeterminate cases on other non-invasive studies and patients with high clinical suspicion (11). Based on the pressures in RHC, PH can be classified and placed in the appropriate group. ICA is particularly useful in the diagnosis of IPAH. RHC also helps in assessing the severity of PH which helps in determining prognosis and predicting response to therapy (25). In RHC, pressures are measured in the RA, RV, PA and PA wedge positions, with oximetry from SVC, IVC, RA, RV, PA and aorta. Cardiac output and index are measured either by angiographic, thermodilution or Fick methods. mPAP is calculated by diastolic PAP + (systolic – diastolic PAP)/3 or [systolic PAP +(2× diastolic PAP)]/3, whereas PVR is calculated as (mPAP – mean PCWP)/cardiac output. mPAP >25 mm at rest (>30 mm at exercise) and PVR >3 Wood units is diagnostic of PAH. Other hemodynamic indices measured include—PVR index, systemic vascular resistance, trans-pulmonary pressure gradient and diastolic pressure gradient (25). Exercise hemodynamic assessment can uncover compensatory mechanisms and identify patients with small vessel disease who may not benefit from surgery (5). In patients with group 1 PH, pulmonary vasoreactivity (PVT) testing may be used to determine if the patients will benefit from calcium channel blockers (11). Vasoreactive patients show a reduction of mPAP ≥10 mmHg to reach absolute values ≤40 mmHg without reduced cardiac output (25,26).

With the routine use of high quality CT pulmonary angiography (CTPA), catheter pulmonary angiography now only has a limited role in the evaluation of thromboembolism. However, this invasive procedure has the highest spatial resolution for evaluating segmental and sub-segmental branches, which is particularly useful in CTEPH to map the vascular and perfusion abnormalities; quantify the severity of PVR; and determine if the vascular abnormalities are amenable for surgery. Centrally located lesions benefit from pulmonary endarterectomy (PEA), whereas peripherally located small vessel lesions/perfusion abnormalities without a central vascular abnormality do not benefit from surgery. Angiographic findings of CTEPH include webs, bands, intimal irregularities, abrupt vascular narrowing, pouching and complete vascular obstruction (*Figure 4*) (27). Angiography also provides a qualitative estimation of pulmonary blood flow and perfusion. Angiography is also used in interventional procedures for CTEPH such as intra-arterial thrombolysis and balloon angioplasty, particularly in patients who may not benefit from PEA. Contraindications include mechanical right sided valves, right sided masses or endocarditis. Complications of angiography include hematoma, pulmonary hemorrhage, pneumothorax, arrhythmia, vasodilation, hypotension and vasovagal reaction.

Computed tomography

CT is a commonly used imaging modality in the evaluation

of PH, due to its high spatial resolution, good field-of-view and multi-planar reconstruction capabilities, although there is risk of radiation and iodinated contrast induced nephrotoxicity. Dilation of the central pulmonary arteries is a common feature of PH. A MPA diameter ≥29 mm has an 89% specificity and 97% PPV in the diagnosis of PH (28) (*Figure 5A*). A diameter smaller than this does not necessarily exclude PH completely, due to its low NPV. If the cut-off is increased to 3.2 cm, the specificity can be increased to 93% and NPV to 90% but the sensitivity decreases to 47% (29). Dilated MPA should be interpreted with caution in patients with ILD, which can cause MPA dilation due to traction without PH and in patients following lung transplantation (30). A ratio of diameter of MPA to that of ascending aorta in the same axial plane of ≥1.0 is also indicative of PH, especially in younger patients (<50) without aortic ectasia, particularly in those with advanced ILD (19,31,32). Segmental artery-to-bronchus diameter ratio of >1:1 in three or four lobes along with dilated MPA has almost 100% specificity in the diagnosis of PH (33). Dilated main right and left pulmonary arteries >18 mm have also been shown to predict mortality (31). An egg and banana sign has been described, with the main pulmonary artery visible at the level of aortic arch (31). In long standing PH, mural calcifications, vascular tortuosity and pruning of peripheral branches may be seen. Tortuosity and fractal dimension correlate with the severity of the PH (34). Dilated MPA may cause extrinsic compression of adjacent structures such as the left main coronary artery (35,36), tracheobronchial tree or recurrent laryngeal nerve (37). Decrease in the pulmonary artery distensibility (<16.5%) on a retrospectively ECG-gated CT is an accurate noninvasive marker of PH, with an 85% sensitivity, 96% specificity (35,38).

Vascular findings are also useful in establishing the cause of PH. Symmetric dilatation of the MPA is a common finding in IPAH compared to CTEPH. Vascular findings of CTPEH include—irregular enlargement of the MPA, webs, bands, intimal irregularities, thrombus with obtuse angle, calcifications, abrupt cut-off, pouch formation, stenosis and post stenotic dilation (*Figure 5B*). CTEPH can be distinguished from acute embolus which forms an acute angle with the vessel wall and expands the vessel and from *in situ* thrombosis which is adherent to the wall and does not have clot retraction, luminal narrowing or pulmonary oligemia/infarcts. Pulmonary artery sarcoma can be distinguished from CTEPH by its acute angle with wall, luminal expansion, nodularity, contrast enhancement and extension to RV, lung or mediastinum (39). Hypertrophied collateral vessels, including bronchial, pleural and intercostal arteries may be seen. Hypertrophied bronchial arteries are associated with hemoptysis and seen at a higher incidence than in IPAH (73% *vs.* 14%) (5,40). CT helps in making a therapeutic decision in CTEPH, based on the clot burden, location and extent. Disease in the main, lobar or proximal segmental arteries may benefit from PEA, whereas distal disease may require medical treatment or balloon angioplasty. PEA in CTEPH patients with dilated bronchial arteries is associated with significantly lower post-operative PVR and mortality rates than those without dilated bronchial arteries (41,42). In the absence of direct visualization of thrombi, indirect signs of chronic PE include disparity in segmental vessel size, mosaic attenuation, parenchymal densities, bronchial collateral arteries, and bronchial dilatation, which are valuable imaging signs to distinguish CTEPH from other causes of PH (42). Higher central arterial dilation, tortuosity and peripheral pruning is seen in CTEPH, correlating with its disease severity (5). There is no dilation of proximal veins or tortuosity in CTEPH and upper lobe predominant pruning is seen in smoking related PH. CTA can also identify vascular anomalies such as anomalous pulmonary venous return or shunts or congenital anomalies as cause of PH. As the pulmonary vascular resistance approaches or exceeds systemic vascular resistance, the shunt may become bidirectional or reversed and is called Eisenmenger syndrome which may be associated with aneurysmal dilatation of the central pulmonary artery and lead to *in situ* calcified thrombus formation (43).

Cardiac findings are seen due to adaptation and subsequent failure of the RV. The RV is hypertrophied (wall thickness >4 mm) and dilated (RV/LV ratio >1) in the axial plane (*Figure 5C*). With retrospective ECG-gated CT, the ventricular volumes (end diastolic and systolic volumes, stroke volumes) and function can be quantified. In cine images, systolic flattening or bowing of the ventricular septum (*Figure 5C*) may be seen with RV pressure elevation (>30 mmHg), which has an 86% sensitivity and 91% specificity for detecting PH (44). A strong correlation is seen between septal bowing and systolic PAP >67 mmHg (45). Increased septal angle correlates with PVR (46). Other significant cardiac predictors for PH include RV free wall ≥6 mm, RV/LV wall ratio ≥0.32, RV/LV lumen ratio ≥1.28, and main PA/ascending aorta ratio ≥0.84 (47). Dilation of the IVC and hepatic veins with contrast reflux also may be present. The RA may also be enlarged, but it is a

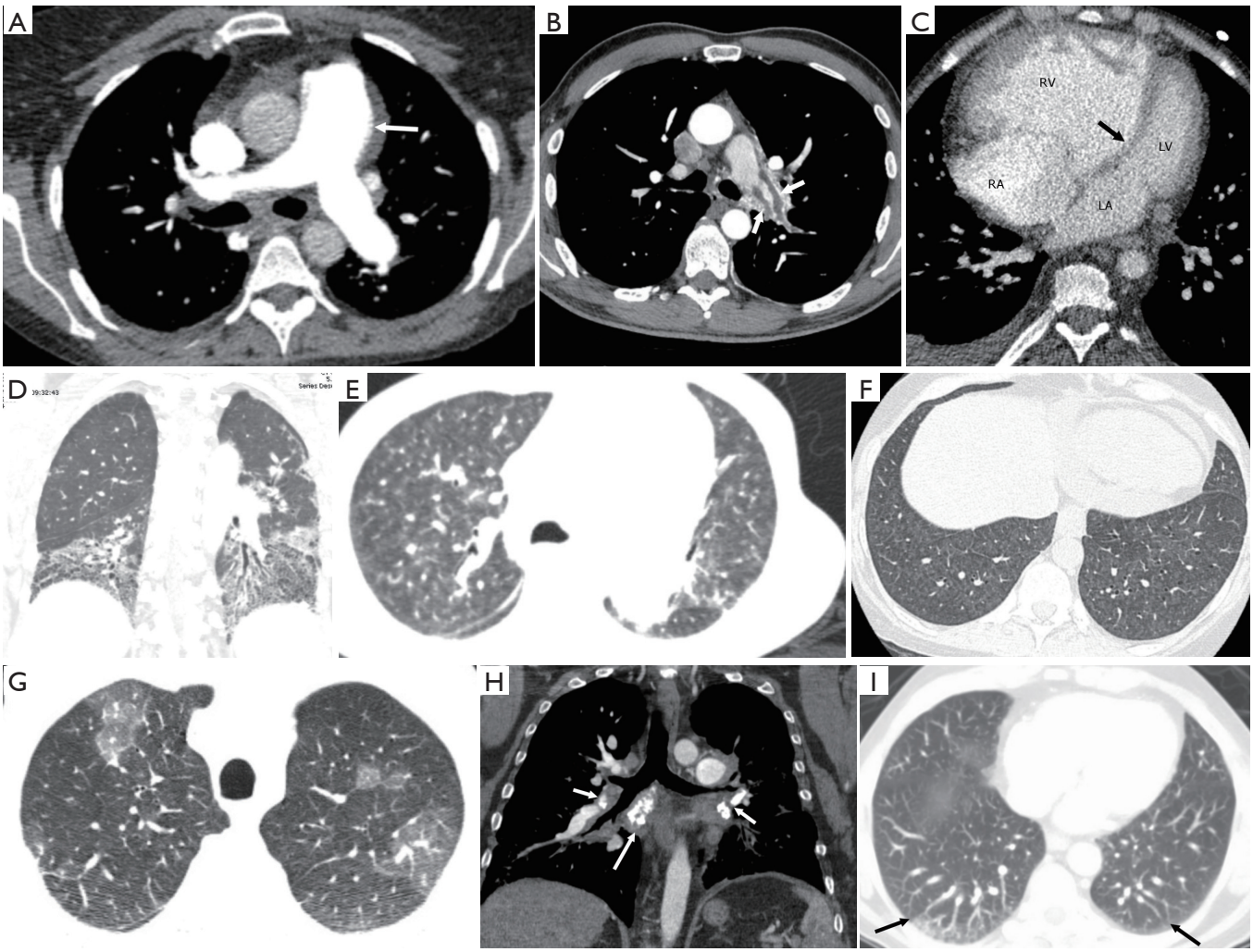

Figure 5 Computed tomography. (A) Axial CT scan at the level of the pulmonary artery bifurcation showing dilation of the main pulmonary artery (arrow), which measures 3.2 cm and measures larger than the ascending aorta at the same level. (B) Axial CT pulmonary angiography shows chronic thrombus (arrows) layering on the wall of the left pulmonary artery. (C) Axial CT scan shows dilation of the RV, compared to the LV, with RV/LV ratio >2.0. The ventricular septum is bowing towards the left (arrow). (D) Coronal high-resolution CT shows bibasal fibrotic changes with architectural distortion, reticulations, traction bronchiectasis and honeycombing in a pattern consistent with usual interstitial pneumonia. (E) Axial high-resolution CT chest in a patient with primary pulmonary arterial hypertension shows multiple centrilobular ground glass nodules, which may represent cholesterol granulomas from recurrent bleeding. (F) Axial CT chest at the level of lung bases shows multiple centrilobular ground glass nodules and smooth interlobular septal thickening in a patient with pulmonary veno-occlusive disease. (G) Axial high-resolution CT scan in a patient with chronic thromboembolic pulmonary hypertension shows alternating areas of high and low attenuation, consistent with mosaic attenuation. Note the small caliber of the vessels in the areas with decreased attenuation compared to the areas with higher attenuation. (H) Coronal CT image in a patient with pulmonary hypertension shows calcified soft tissue densities in the hilar and subcarinal regions (arrows) with peribronchial thickening of the right middle lobe bronchus secondary to fibrosing mediastinitis. (I) Axial CT scan in a patient with portal hypertension and hepatopulmonary syndrome shows dilated peripheral pulmonary arterial branches in the posterior lower lobes (arrows), which are extending till the pleural surface. RA, right atrium; LA, left atrium; RV, right ventricle; LV, left ventricle.

non-specific finding for PH, as it is also seen in tricuspid insufficiency. Pericardial effusion may be seen. Cardiac CT also allows the evaluation of CHD, including shunts. It is particularly useful in the evaluation of defects that are difficult to detect by TTE such as sinus venosus defects, which have a high association with partial anomalous venous return of the pulmonary veins (48). Cardiac CT is useful in evaluating the left heart and possible causes of PH in group 2, including mitral annular calcifications, aortic stenosis with calcification and different types of cardiomyopathies of ischemic or non-ischemic origin (48). Pericardial effusion may be seen, which in the context of PH usually indicates worsening of the disease (49).

Lung parenchymal findings, especially with the use of high resolution chest CT (HRCT) can help in establishing the etiology of PH, particularly COPD and ILD (*Figure 5D*), which may be idiopathic or associated with connective tissue disease, sarcoidosis, and pulmonary Langerhans cell histiocytosis (50,51). Dilatation of the esophagus can suggest the diagnosis of scleroderma as a cause of lung disease and PH. Combined pulmonary fibrosis and emphysema seems to have a high association and prevalence of PH which also determines the morbidity and mortality in these patients (52-54). A common finding seen in patients with IPAH is large diffusely distributed ill-defined centrilobular ground-glass nodules (55), which correspond to cholesterol granulomas secondary to ingestion of red blood cells by pulmonary macrophages (56) (*Figure 5E*). Differential diagnosis includes hypersensitivity pneumonitis, respiratory bronchiolitis, follicular bronchiolitis and long-standing L-R shunt. Centrilobular ground-glass nodules along with tortuous corkscrew vessels can also be seen in patients with PCH (57,58) and PVOD, which have overlapping features. Ground glass nodules in PCH are larger than the typical centrilobular nodules as well as PVOD nodules (5). Ground glass nodules in PVOD can be centrilobular, patchy, geographic, diffuse, mosaic or perihilar and associated with smooth interlobular septal thickening, pleural effusions, and lymphadenopathy (59,60) (*Figure 5F*).

Parenchymal findings of CTEPH include focal atelectasis and scars from prior infarcts, pleural thickening and mosaic attenuation (*Figure 5G*). Infarcts are seen as peripheral wedge-shaped density, with internal lucencies, truncated apex and feeding vessel leading to it. Mosaic attenuation pattern refers to alternating areas of high and low attenuation, which is seen in CTEPH as well as other causes of PH. The low attenuation areas represent hypoperfusion and high attenuation areas represent vascular redistribution and collaterals. Four patterns of mosaic attenuation are identified and may be used to differentiate various groups of PH. For example, a pattern associated with central hyper attenuation and peripheral hypoattenuation was found more frequently in groups 1 and 4 (26). Mosaic attenuation can also be seen in small airway disease. In PH, the vasculature in the dark areas is smaller than the bright areas, whereas in small airway disease, they are similar size and there is air trapping in expiratory images (54). Cylindrical bronchiectasis in segmental and subsegmental bronchi may be seen in CTEPH due to hypoxia adjacent to thrombosed vessels (61).

Fibrosing mediastinitis is a rare condition that may manifest as calcified or non-calcified soft tissue narrowing of the central airways, pulmonary arteries or veins secondary to fibrotic reaction induced by granulomatous infection (62) (*Figure 5H*). Tumor emboli from renal, hepatocellular and breast cancer can cause PH and are seen as intravascular filling defects in the central pulmonary arteries or as multifocal beading and dilatation of the peripheral pulmonary arteries on CT with contrast. Pulmonary talcosis secondary to injection of crushed oral medication into peripheral veins can block the pulmonary arterioles, resulting in fine, diffuse centrilobular ground glass nodules associated with dilated MPA and RV. Takayasu arteritis may involve the main pulmonary artery in 50–80% of patients as manifestation of late-stage disease (63) and manifests as vascular thickening, delayed contrast enhancement, aneurysms and stenosis. Liver cirrhosis and portal hypertension may lead to hepatopulmonary shunts, seen as dilated and tortuous peripheral subsegmental vessels (*Figure 5I*) (64).

Technical advances

Due to technological advances, it is now possible to obtain high quality CT images at low doses of radiation as well as iodinated contrast media. Radiation doses are minimized by using the least possible tube voltage and tube current that provides diagnostic image quality. Noise, which used to be a limitation of low-radiation dose studies can be minimized by using advanced iterative reconstruction algorithms. Low tube voltage also helps in minimizing contrast dose, since at low tube voltage the K-edge of iodine is approximated, as a result of which there is increased photoelectric attenuation. High-pitch helical mode is now possible in the latest generation dual source scanners, which helps in rapid acquisition, with the inherent gaps in data filled by data from the second X-ray tube. This technique has low

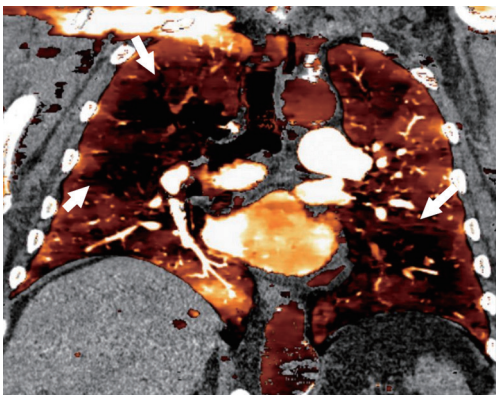

Figure 6 Dual energy CT. Coronal dual-energy CT perfusion map in a patient with pulmonary hypertension shows multiple areas of perfusion defects throughout the lungs (arrows)

motion artifact and also facilitates the use of low radiation and contrast doses. CTPA has been performed with contrast as low as 20 mL and radiation dose below 1 mSv without degradation of image quality (65,66). There are also other wide-array scanners, which cover a large anatomical area of the patient in one acquisition (up to 16 cm), which also helps in reducing motion, radiation and contrast.

Dual energy CT

Dual-energy CT (DECT) (aka spectral CT, multi-energy CT) is also increasingly used in PH. In this CT technique, images are obtained at two distinct energy levels. Using differential interactions of materials at different energy levels, additional material-specific information is obtained. Currently there are several technologies of DECT including dual source, rapid kVp switching, dual layer, dual spin, split beam and photon counting technologies. Spectral images include iodine maps, virtual non-contrast (VNC), virtual monoenergetic images (VMI) and effective atomic number-based images. From post-contrast CT angiographic images, automatic perfusion blood volume (PBV) maps of the lungs can be generated by using a three-material decomposition process. This is not a true perfusion scan, since the image is obtained in one single time point. Perfusion is color coded for lung parenchymal tissues between –960 and –600 HU and can also be fused with conventional images to provide combined assessment.

In PH, DECT provides comprehensive information on several facets of the disease, including morphological information on vasculature and functional information on perfusion. Although PBV map differs in mechanism from a V/Q scan (also V/Q is performed in shallow breathing, PBV in full inspiration), multiple studies have shown good correlation between these imaging techniques, with one study showing a 99% specificity and 83% sensitivity on a per-segment level (67). Another study showed 96% sensitivity and 76% specificity when compared with SPECT (68). In CTEPH, heterogeneous perfusion defects are seen in the PBV maps (*Figure 6*), similar to the mosaic attenuation seen in the lung window (69). The perfusion defects may or may not correspond to lesions in the supplying arteries such as webs, bands, stenosis or occlusion. Occasionally perfusion defects are the only findings without vascular abnormalities, either due to small thrombi beyond the resolution of CT or due to recanalization (70). Perfusion defects in segments supplied by abnormal vasculature usually respond to PEA, while poor results are seen in perfusion defects without vascular abnormalities (69). Occasionally, there may be residual perfusion distal to an occluded vascular segment, likely due to bronchial collaterals, which can be identified by using a threshold value of 20 HU. These patients also respond well to PEA (71). The perfusion defects of CTEPH can be distinguished from that of acute PE, which is usually segmental and wedge shaped. Like a nuclear V/Q scan, the defects are mismatched, with no corresponding parenchymal abnormality seen in the lung windows or ventilation DECT with Xenon. However, these defects may correlate with dark areas of mosaic attenuation in the lung window, which is seen in CTEPH, other causes of PH and small airway disease. Small airway disease can be distinguished based on the presence of air trapping in expiratory images, less size variation between the dark and bright areas and less pronounced vascular perfusion defect resulting in discordance with the extent of hypoattenuation. CTEPH has a concordant perfusion defect that matches with the hypoattenuation (72). Presence of higher iodine content in the bright areas of mosaic attenuation also indicates a vascular cause than airway abnormality (73). Other causes of PH also show perfusion defects due to vascular endothelial damage, vasoconstriction and cellular proliferation (69). While CTEPH shows large, multiple, segmental or sub-segmental, well-defined perfusion defects, IPAH shows small, non-segmental, inhomogeneous, mottled, patchy defects (74,75). Other abnormalities such as ILD, emphysema and small airway disease also cause perfusion defects, but these can be distinguished from CTEPH by correlating with lung windows. Artefactual defects can be

Table 2 MRI sequences used in pulmonary hypertension

Sequence	Utility
Black blood double inversion recovery	Morphology
Cine imaging	Morphology, function, volumes
Strain imaging	Regional myocardial function
Velocity encoded phase contrast	Flow, pressure, hemodynamics
Late gadolinium enhancement	Establishing etiology, prognosis
T1, T2 mapping	Fibrosis, edema, prognosis
MR angiography	Vascular abnormalities, perfusion
MR perfusion imaging (contrast, arterial spin labeling)	Lung perfusion

MRI, magnetic resonance imaging.

caused by motion and beam hardening.

Quantitative analysis of the lung perfusion can also be performed. While some earlier studies did not show correlation between PBV and PVR (71), other studies have shown good correlation with mPAP and PVR in PH (76,77). In PH, there is higher central than peripheral enhancement, decreased global parenchymal enhancement due to delayed parenchymal transit (69) and greater variation in parenchymal enhancement. There is correlation of ratio of central/parenchymal enhancement with the PVR (69). By obtaining DECT in two phases, acute PE can be distinguished from chronic PE, since in chronic PE more enhancement is seen in the delayed phase due to presence of bronchial collaterals (78). There is potential for evaluating myocardial ischemia of the RV using DECT (69), which is still at earlier stages. Virtual non-contrast images can be used to evaluate for the calcifications seen in the pulmonary arterial wall in chronic PH, which can be obscured by contrast (69). VMI at low energy levels can be used to improve the contrast signal, which can be prospectively used to lower contrast doses, improve visualization of peripheral branches and collaterals, retrospectively salvage suboptimal studies. VMI at high energy levels can be used to minimize some artifacts, particularly beam hardening which can be seen due to dense contrast in the SVC.

Magnetic resonance imaging

MRI has several advantages in the evaluation of PH, including good spatial resolution, high temporal resolution, wide field-of-view, multi-planar imaging and tissue characterization capabilities. It is useful in diagnosis, establishing etiology, quantification including hemodynamics, prognostication and follow-up after treatment. Several MRI sequences are available for the evaluation of PH, which are listed in *Table 2*.

In PH, MRI shows dilated central pulmonary arteries which can be evaluated in black blood, bright blood SSFP sequences or MR angiography (*Figure 7A*). MPA diameter of ≥29 mm or ratio of MPA and ascending aortic diameter >1 are used in the diagnosis. The presence of intraluminal hyperintensity in black-blood images due to slow flow artifact indicates PH with estimated mPAP >70 mm and high PVR (79,80). On velocity-encoded phase contrast images, low velocity in the main pulmonary artery (i.e., <11.7 cm/s) and early retrograde flow are suggestive of PH, with the former having a 92.9% sensitivity and 82.4% specificity (81). Elevated pulse wave velocity may also be demonstrated in the central pulmonary arteries. With 4D flow, turbulent vortex is seen in the central pulmonary arteries, the duration of which correlates directly with mPAP (82).

Secondary cardiac changes of PH include RV dilation and hypertrophy (*Figure 7B*). RV dilation is diagnosed in axial images when the RV:LV diameter >1. RV hypertrophy is diagnosed when then RV wall thickness >4 mm. Ventricular mass ratio (RV/LV mass) >0.6 has 84% sensitivity and 71% specificity in the diagnosis of PH (21,22). The normally rightward-convex ventricular septum is either flattened or bowed towards the LV during systole. As a result, the LV becomes D-shaped and the RV becomes progressively concentric (83). There is a strong correlation between the measurement of the paradoxical curvature of the interventricular septum and the severity of PH (45). RV ejection fraction diminishes as a result of the septal bowing. Late gadolinium enhancement (LGE) is often seen in the septum at the RV insertion sites due to pressure overload resulting in structural deformation from mechanical strain. Correspondingly, elevated T1 values can be seen in T1 mapping sequences. With time-resolved MR Angiography, increased pulmonary transit time may be seen. Increased RV mass, decreased RV function (<35%) and prolonged vertical flow indicate RV failure (82).

MRI is also valuable in evaluating the etiology of PH. Several cardiomyopathies can be diagnosed using the morphology and LGE patterns in MRI, with ischemic disorders showing subendocardial to transmural pattern

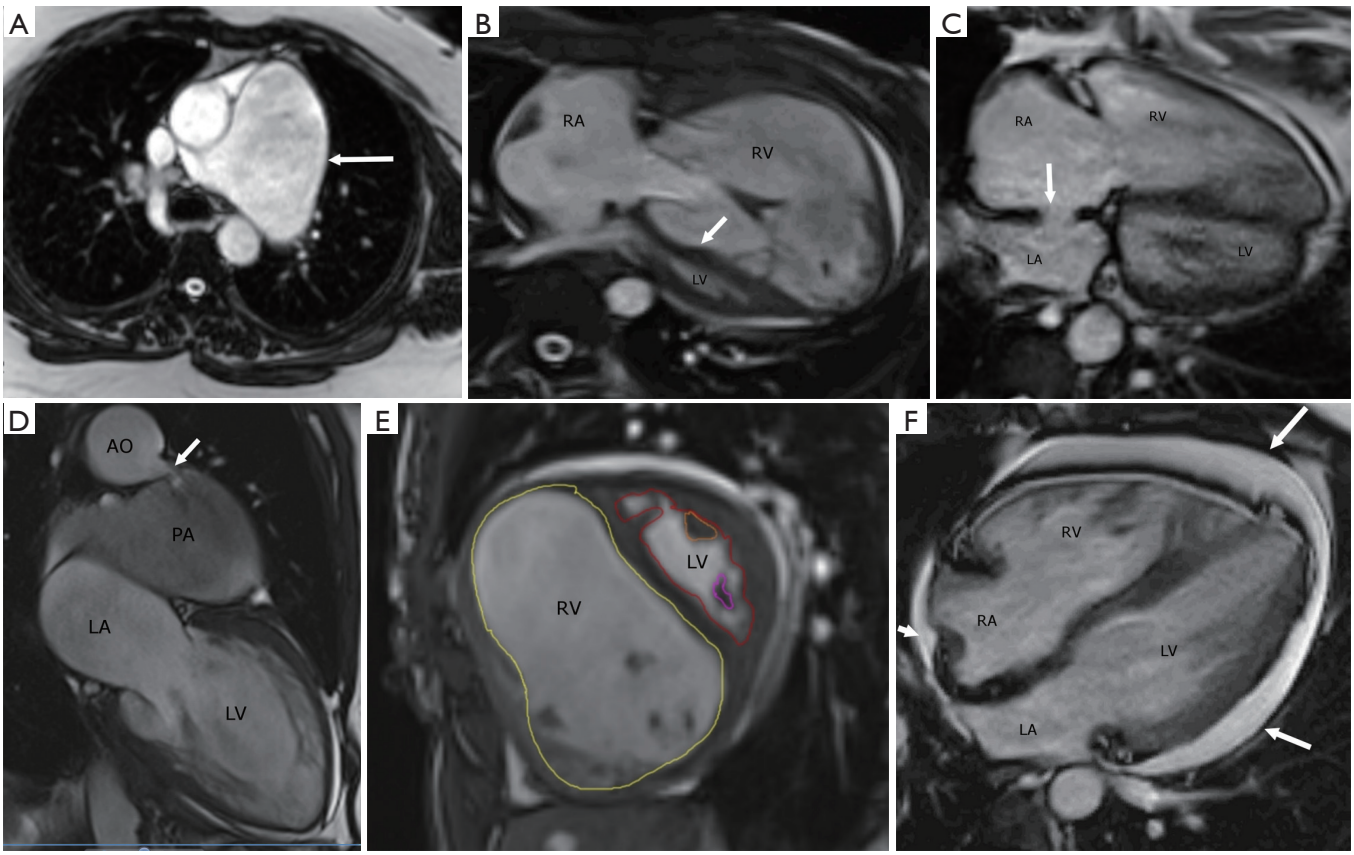

Figure 7 Magnetic resonance imaging. (A) Axial steady state free precession image (SSFP) shows severe dilation of the main pulmonary artery (arrow). (B) Axial SSFP image shows severe dilation and hypertrophy of the right ventricle (RV), with decreased size of the left ventricle (LV). The interventricular septum is flattened and bowed to the left (arrow). (C) Axial SSFP image shows a moderate-sized secundum type of atrial septal defect (arrow). Note the enlargement of the right ventricle and right atrium with flattening of the ventricular septum. (D) Two-chamber SSFP image shows a patent ductus arteriosus (arrow) connecting the aortic arch (AO) and a dilated left pulmonary artery (PA). (E) Short axis SSFP MRI image shows quantification of the RV by drawing endocardial contour in the end-diastolic image (yellow contour) and quantification of the LV by an endocardial contour in the end-diastolic image (red contour). (F) Axial SSFP image in a patient with pulmonary hypertension shows a moderate-sized circumferential pericardial effusion (arrows). Note also the dilated and hypertrophied right ventricle (RV). RA, right atrium; LA, left atrium.

and non-ischemic entities showing various patterns of mid-myocardial, sub-epicardial or global subendocardial patterns of enhancement. Other cardiac causes of PH can also be evaluated including CHDs (*Figure 7C,D*), and valvular disorders. MRI is not the primary modality for the evaluation of lung disorders, but some lung disorders are evident in MRI. Delayed enhancement MRI has been shown to demonstrate fibrosis in interstitial lung disease (84). Vascular disorders can be evaluated using MR Angiography and MR perfusion, including time-resolved sequences. In CTEPH, areas of webs, bands, irregularities, narrowing, pouching, obstruction and post-stenotic dilation are seen in MRA. MR perfusion can show perfusion defects, with good correlation with scintigraphy (85). Using indicator dilution theory, mean transit time, time to peak and blood volume can be estimated, although true quantitative perfusion is not achieved. Arterial spin labelling or Fourier decomposition can also evaluate for perfusion without the need for intravenous or inhaled contrast agents (86,87).

MRI is an ideal tool for providing several quantitative metrics in PH. MRI is the gold standard in the quantification of ventricular volumes and function, with echocardiography limited in the evaluation of RV due to is complex shape and morphology, particularly in patients

with limited acoustic windows such as obesity, chest wall deformities or COPD.

RV quantification is valuable in assessment of disease severity and monitoring response to therapy. RV quantification can be performed in the axial (88), as well as short axis planes (89-91) (*Figure 7E*). RV function can also be evaluated by TAPSE, the displacement of the lateral tricuspid annular plane between end-diastole and end-systole. Normal TAPSE is >15 mm, with RV dysfunction showing values <10 mm. Strain imaging techniques such as tagging, feature tracking, sensitivity encoding (SENC), phase contrast and DENSE evaluate for regional function. RV strain has been shown to be associated with disease severity and independently associated with poor outcomes (92). Eccentricity index is measured by dividing the antero-posterior (AP) intra-cavitary diameter (D2) of the LV by the septal-lateral diameter (D1), with normal value of 1. In PH, the eccentricity index is >1, indicative of worse prognosis (93). In cardiac shunts, the ratio of pulmonary to systemic circulation (Qp/Qs) can be measured using phase-contrast velocity-encoded sequences. A ratio >1 indicates left-to-right shunt, with ratios of 1.7–2.0 used for determining the need for surgical intervention. A ratio <1 indicates a right-to-left shunt. Qp is measured at the level of the pulmonary artery and Qs at the level of ascending aorta. For shunts located in the heart, such as atrial and ventricular septal defects, this measurement holds true. For shunts that are distal to these sites of flow measurement (e.g., patent ductus arteriosus, aorto-pulmonary window), Qs represents the pulmonary flow and Qp represents the systemic flow.

MRI can provide several non-invasive metrics that reflect the hemodynamics of the pulmonary arterial system, although with not the same accuracy. The curvature of the ventricular septum shows strong correlation with the RV-LV pressure gradient and is comparable to the RV systolic pressure in RHC (94,95). The angle of maximal septal excursion into the LV in ventricular systole, i.e., interventricular angle (α) also shows a strong correlation with invasive mPAP (20). The mPAP and PVR can also be estimated in MRI by using regression equations. Estimated mPAP = (α ×0.23) + (ventricular mass index ×16.3)–4.6. This estimated mPAP has a sensitivity of 87% and specificity of 90% in diagnosing PH >32 mmHg. Since, PVR is the maximal change in flow rate during ejection/acceleration volume, it can be estimated in Woods units by the formula 19.38–[4.62× ln PA average velocity (cm/s)] – [0.08× RVEF(%)] (96). Correlation has also been shown between the velocity of the flow in pulmonary artery and the pressure. Other indices used in PH include—decreased relative change of area; increased Vmax; increased time to Vmax; maximal change in flow at ejection time; decreased windkessel effect; increased oscillatory shear index; increased shear range index; transpulmonary gradient in pulmonary artery; transmitral flow; myocardial tissue velocity; left atrial volume and flow.

MRI allows for estimation of prognostic factors and risk stratification. For example, the volume of LGE correlates with the RV mass, RV volume, RV dysfunction, RV remodeling and septal curvature, indicating adverse prognosis (94,97,98). Cardiac output in phase contrast MRI is also an independent adverse prognostic factor. There is also a negative correlation between the average velocity in the MPA and the mPAP (81). Presence of slow flow in the main pulmonary artery correlates with poor prognosis and mortality (94). Elevated PA stiffness impacts ventriculo-arterial coupling resulting in greater RV afterload. Pulmonary artery stiffness also predicts mortality, associated with mPAP and PVR. Distensibility of the pulmonary artery, i.e., the difference in cross sectional area of pulmonary artery between end-diastole and end-systole of >10% indicates good response to vasodilator therapy (99), whereas compliance of <16% has been shown to have poor prognosis (100). Presence of pericardial effusion is also an adverse prognostic factor (49) (*Figure 7F*).

MRI is also used in the follow up of treatment and assessment of response to therapy. If the therapy is successful, the mPAP, RV mass, EDV and ESV decrease, while the EF increases, typically in 3 months (101). The change in RV function is an independent predictor of mortality, independent of clinical and other hemodynamic factors (1,19). The septal bowing may also decrease with the use of vasodilators. Limitations of MRI include its cost, limited availability, need for higher expertise, long scan time and contraindications including metallic devices and gadolinium contrast media in patients with severe renal dysfunction.

Diagnostic algorithm for PH

The work-up of PH involves four steps—suspicion, detection, classification and functional evaluation (102). High index of suspicion for PH should be present in patients with exertional limitation in cardiac output,

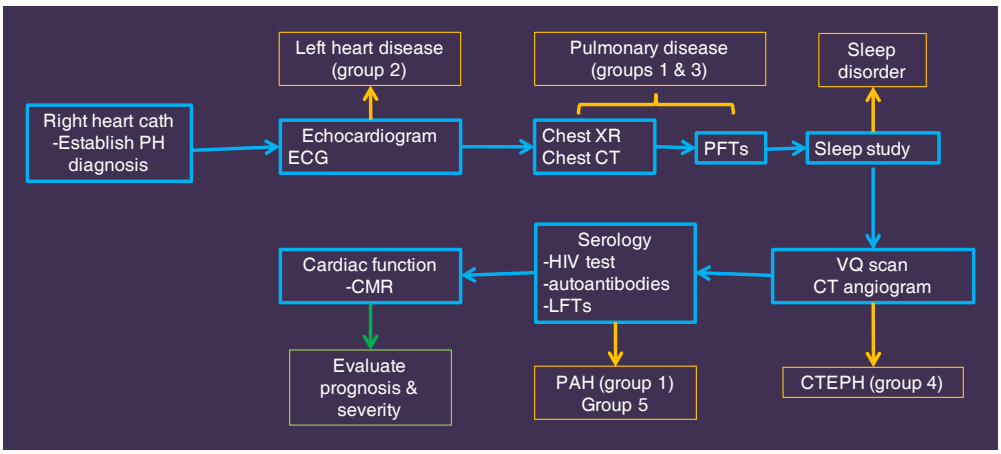

Figure 8 Diagnostic algorithm. A flow chart showing the typical management of patients with pulmonary hypertension at our institution.

particularly in young patients with connective tissue disease, CHD, and history of PE. Echocardiogram is the initial imaging test used in all the patients. Doppler measured PASP is used to determine the probability of PH, with a sensitivity of 79–100% and a specificity of 68–98% (9,103). PH can also be diagnosed in the other non-invasive imaging tests as described above. The definitive diagnosis of PH and its severity is established before treatment by RHC measurement of mPAP, PVR and PCWP. Multiple tests, including imaging are then used to establish the etiology of PH (11). TTE is useful in evaluating group 2 disorders. Chest radiograph, CT and pulmonary function tests and sleep studies are performed for evaluating pulmonary and hypoxic disorders (groups 1 and 3). V/Q scan and/or CT angiogram are used for evaluating CTEPH (group 4). Serology including HIV test, autoantibodies and liver function tests are used for diagnosing PAH (group 1) or miscellaneous disorders (group 5). MRI or CT can be used for evaluating CHD. PET/CT or PET/MRI can be used for diagnosing pulmonary arteritis or neoplasm. When all these conditions are excluded, a diagnosis of IPAH can be established. Cardiac MRI is the gold standard in the quantification of RV volumes and function, which is useful for prognosis, treatment monitoring and evaluating response to therapy (9,104). MRI can also provide some non-invasive pulmonary hemodynamics, since it is impractical to perform serial catheterizations for follow-up. Catheter pulmonary angiography is reserved for those patients who require thrombolysis or balloon angioplasty for CTEPH and pre-surgical evaluation before PEA. An algorithm used in our institute for PH is described in *Figure 8*.

Conclusions

Imaging plays a vital role in the evaluation of PH, including diagnosis, establishing etiology, quantification, risk stratification and assessment of therapeutic response.

Acknowledgements

None.

Footnote

Conflicts of Interest: The authors have no conflicts of interest to declare.

References

1. Hyduk A, Croft JB, Ayala C, et al. Pulmonary hypertension-surveillance- United States. MMWR Surveill Summ 2005;54:1-28.
2. Hoeper MM, Gibbs SR. The changing landscape of pulmonary arterial hypertension and implications for patient care. Eur Respir Rev 2014;23:450-7.
3. Badesch DB, Champion HC, Sanchez MA, et al. Diagnosis and assessment of pulmonary arterial hypertension. J Am Coll Cardiol 2009;54:S55-66.
4. Simonneau G, Gatzoulis MA, Adatia I, et al. Updated clinical classification of pulmonary hypertension. J Am Coll Cardiol 2013;62:D34-41.
5. Renapurkar RD, Shrikanthan S, Heresi GA, et al. Imaging in Chronic Thromboembolic Pulmonary Hypertension. J Thorac Imaging 2017;32:71-88.

6. Goldberg AB, Mazur W, Kalra DK. Pulmonary hypertension: diagnosis, imaging techniques and novel therapies. Cardiovasc Diagn Ther 2017;7:405-17.
7. Lang IM, Plank C, Sadushi-Kolici R, et al. Imaging in pulmonary hypertension. JACC Cardiovasc Imaging 2010;3:1287-95.
8. Farber HW, Loscalzo J. Pulmonary arterial hypertension. N Engl J Med 2004;351:1655-65.
9. Peña E, Dennie C, Veinot J, et al. Pulmonary hypertension: how the radiologist can help. Radiographics 2012;32:9-32.
10. Rich S, Dantzker DR, Ayres SM, et al. Primary pulmonary hypertension. A national prospective study. Ann Intern Med 1987;107:216-23.
11. Expert Panel on Thoracic Imaging, Sirajuddin A, Donnelly EF, et al. ACR Appropriateness Criteria® Suspected Pulmonary Hypertension. J Am Coll Radiol 2017;14:S350-61.
12. Miniati M, Monti S, Airo E, et al. Accuracy of chest radiography in predicting pulmonary hypertension: a case-control study. Thromb Res 2014;133:345-51.
13. Galiè N, Humbert M, Vachiery JL, et al. 2015 ESC/ERS Guidelines for the diagnosis and treatment of pulmonary hypertension: The Joint Task Force for the Diagnosis and Treatment of Pulmonary Hypertension of the European Society of Cardiology (ESC) and the European Respiratory Society (ERS): Endorsed by: Association for European Paediatric and Congenital Cardiology (AEPC), International Society for Heart and Lung Transplantation (ISHLT). Eur Heart J 2016;37:67-119.
14. Otto CM. editor. The practice of clinical echocardiography. Elsevier Health Sciences, 2012:634.
15. Grapsa J, O'Regan DP, Pavlopoulos H, et al. Right ventricular remodelling in pulmonary arterial hypertension with three-dimensional echocardiography: comparison with cardiac magnetic resonance imaging. Eur J Echocardiogr 2010;11:64-73.
16. Tei C, Ling LH, Hodge DO, et al. New index of combined systolic and diastolic myocardial performance: a simple and reproducible measure of cardiac function- a study in normals and dilated cardiomypathy. J Cardiol 1995;26:357-66.
17. Armstrong WF, Ryan T. editors. Figenbaum's Echocardiography. 7th ed. Philadelphia, OA: Lippincott Williams and Wilkins, 2009.
18. Oudiz RJ. Pulmonary hypertension associated with left-sided heart disease. Clin Chest Med 2007;28:233-41.
19. Ng CS, Wells AU, Padley SP. A CT sign of chronic pulmonary arterial hypertension: the ratio of main pulmonary artery to aortic diameter. J Thorac Imaging 1999;14:270-8.
20. Ley S, Ley-Zaporozhan J, Pittonn MB, et al. Diagnostic perfformmance oftaof-thee-art imaging techniques for morphological assessmmennt of vaascular abnormalities in patieentss with chronic thromboembollic pulmonary hypertension (CTEPH). Eur Radiol 2012;22:607-16.
21. Ascha M, Renapurkar RD, Tonelli AR. A review of imaging modalities in pulmonary hypertension. Ann Thorac Med 2017;12:61-73.
22. Giordano J, Khung S, Duhamel A, et al. Lung perfusion characteristics in pulmonary arterial hypertension (PAH) and peripheral forms of chronic thromboembolic pulmonary hypertension (pCTEPH): Dual-energy CT experience in 31 patients. Eur Radiol 2017;27:1631-9.
23. Lau EM, Bailey DL, Bailey EA, et al. Pulmonary hypertension leads to a loss of gravity dependent redistribution of regional lung perfusion: a SPECT/CT study. Heart 2014;100:47-53.
24. Tatebe S, Fukumoto Y, Oikawa-Wakayama M, et al. Enhanced [18F]fluorodeoxyglucose accumulation in the right ventricular free wall predicts long-term prognosis of patients with pulmonary hypertension: a preliminary observational study. Eur Heart J Cardiovasc Imaging 2014;15:666-72.
25. Rosenkranz S, Preston IR. Right heart catheterization: best practice and pitfalls in pulmonary hypertension. Eur Respir Rev 2015;24:642-52.
26. Grothues F, Smith GC, Moon JC, et al. Comparison of interstudy reproducibility of cardiovascular magnetic resonance with two-dimensional echocardiography in normal subjects and in patients with heart failure or left ventricular hypertrophy. Am J Cardiol 2002;90:29-34.
27. Auger WR, Fedullo PF, Moser KM, et al. Chronic major-vessel thromboembolic pulmonary artery obstruction: appearance at angiography. Radiology 1992;182:393-8.
28. Tan RT, Kuzo R, Goodman LR, et al. Utility of CT scan evaluation for predicting pulmonary hypertension in patients with parenchymal lung disease. Medical College of Wisconsin Lung Transplant Group. Chest 1998;113:1250-6.
29. Alhamad EH, Al-Boukai AA, Al-Kassimi FA, et al. Prediction of pulmonary hypertension in patients with or without interstitial lung disease: reliability of CT findings. Radiology 2011;260:875-83.
30. Devaraj A, Wells AJ, Meister MG, et al. The effect of diffuse pulmonary fibrosis on the reliability of CT signs of

pulmonary hypertension. Radiology 2008;249:1042-9.
31. Devaraj A, Hansell DM. Computed tomography signs of pulmonary hypertension: old and new observations. Clin Radiol 2009;64:751-60.
32. Devaraj A, Wells AU, Meister MG, et al. Detection of pulmonary hypertension with multidetector CT and echocardiography alone and in combination. Radiology 2010;254:609-16.
33. Frazier AA, Burke AP. The imaging of pulmonary hypertension. Semin Ultrasound CT MR 2012;33:535-51.
34. Helmberger M, Pienn M, Urschler M, et al. Quantification of torusity and fractal dimension of the lung vessels in pulmonary hypertension patients. PLoS One 2014;9:e87515.
35. Revel MP, Faivre JB, Remy-Jardin M, et al. Pulmonary hypertension: ECG-gated 64-section CT angiographic evaluation of new functional parameters as diagnostic criteria. Radiology. Radiology 2009;250:558-66.
36. Kawut SM, Silvestry FE, Ferrari VA, et al. Extrinsic compression of the left main coronary artery by the pulmonary artery in patients with long-standing pulmonary hypertension. Am J Cardiol 1999;83:984-6, A10.
37. Mesquita SM, Castro CR, Ikari NM, et al. Likelihood of left main coronary artery compression based on pulmonary trunk diameter in patients with pulmonary hypertension. Am J Med 2004;116:369-74.
38. Zisman DA, Karlamangla AS, Ross DJ, et al. High-resolution chest CT findings do not predict the presence of pulmonary hypertension in advanced idiopathic pulmonary fibrosis. Chest 2007;132:773-9.
39. Chong S, Kim TS, Kim BT, et al. Pulmonary artery sarcoma mimicking pulmonary thromboembolism: integrated FDG PET/CT. AJR Am J Roentgenol 2007;188:1691-3.
40. Remy-Jardin M, Duhamel A, Deken V, et al. Systemic collateral supply in patients with chronic thromboembolic and primary pulmonary hypertension: assessment with multi-detector row helical CT angiography. Radiology 2005;235:274-81.
41. Castañer E, Gallardo X, Ballesteros E, et al. CT diagnosis of chronic pulmonary thromboembolism. Radiographics 2009;29:31-50.
42. Kauczor HU, Schwickert HC, Mayer E, et al. Spiral CT of bronchial arteries in chronic thromboembolism. J Comput Assist Tomogr 1994;18:855-61.
43. Dakkak W, Tonelli AR. Compression of adjacent anatomical structures by pulmonary artery dilation. Postgrad Med 2016;128:451-9.
44. Alunni JP, Degano B, Arnaud C, et al. Cardiac MRI in pulmonary artery hypertension: correlations between morphological and functional parameters and invasive measurements. Eur Radiol 2010;20:1149-59.
45. Roeleveld RJ, Marcus JT, Faes TJ, et al. Interventricular septal configuration at mr imaging and pulmonary arterial pressure in pulmonary hypertension. Radiology 2005;234:710-7.
46. Liu M, Ma ZH, Guo XJ, et al. A septal angle measured on computed tomographic pulmonary angiography can non-invasively estimate pulmonary vascular resistance in patients with chronic thromboembolic pulmonary hypertension. J Thorac Imaging 2012;27:325-30.
47. Chan AL, Juarez MM, Shelton DK, et al. Novel computed tomographic chest metrics to detect pulmonary hypertension. BMC Med Imaging 2011;11:7.
48. Lewis G, Hoey ET, Reynolds JH, et al. Multi-detector CT assessment in pulmonary hypertension: techniques, systematic approach to interpretation and key findings. Quant Imaging Med Surg 2015;5:423-32.
49. Sahay S, Tonelli AR. Pericardial effusion in pulmonary arterial hypertension. Pulm Circ 2013;3:467-77.
50. Perloff JK, Hart EM, Greaves SM, et al. Proximal pulmonary arterial and intrapulmonary radiologic features of Eisenmenger syndrome and primary pulmonary hypertension. Am J Cardiol 2003;92:182-7.
51. Ryu JH, Krowka MJ, Pellikka PA, et al. Pulmonary hypertension in patients with interstitial lung diseases. Mayo Clin Proc 2007;82:342-50.
52. Ley S, Kreitner KF, Fink C, et al. Assessment of pulmonary hypertension by CT and MR imaging. Eur Radiol 2004;14:359-68.
53. Hirano AC, Targueta EP, Ferraz de Campos FP, et al. Severe pulmonary hypertension due to combined pulmonary fibrosis and emphysema: another cause of death among smokers. Autops Case Rep 2017;7:15-26.
54. Ridge CA, Bankier AA, Eisenberg RL. Mosaic attenuation. AJR Am J Roentgenol 2011;197:W970-7.
55. Horton MR, Tuder RM. Primary pulmonary arterial hypertension presenting as diffuse micronodules on CT. Crit Rev Comput Tomogr 2004;45:335-41.
56. Thabut G, Dauriat G, Stern JB, et al. Pulmonary hemodynamics in advanced COPD candidates for lung volume reduction surgery or lung transplantation. Chest 2005;127:1531-6.
57. Edwards PD, Bull RK, Coulden R. CT measurement of main pulmonary artery diameter. Br J Radiol 1998;71:1018-20.

58. Nolan RL, McAdams HP, Sporn TA, et al. Pulmonary cholesterol granulomas in patients with pulmonary artery hypertension: chest radiographic and CT findings. AJR Am J Roentgenol 1999;172:1317-9.
59. Lantuéjoul S, Sheppard MN, Corrin B, et al. Pulmonary veno-occlusive disease and pulmonary capillary hemangiomatosis: a clinicopathologic study of 35 cases. Am J Surg Pathol 2006;30:850-7.
60. Montani D, Achouh L, Dorfmuller P, et al. Pulmonary veno-occlusive disease: clinical, functional, radiologic, and hemodynamic characteristics and outcome of 24 cases confirmed by histology. Medicine (Baltimore) 2008;87:220-33.
61. Wetzel RC, Herold CJ, Zerhouni EA. Hypoxic bronchodilation. J Appl Physiol 1992;73:1202-6.
62. Soler X, Hoh CK, Test VJ, et al. Single photon emission computed tomography in chronic thromboembolic pulmonary hypertension. Respirology 2011;16:131-7.
63. Matsunaga N, Hayashi K, Sakamoto I, et al. Takayasu arteritis: protean radiologic manifestations and diagnosis. Radiographics 1997;17:579-94.
64. McAdams HP, Erasmus J, Crockett R, et al. The hepatopulmonary syndrome: radiologic findings in 10 patients. AJR Am J Roentgenol 1996;166:1379-85.
65. Bucher AM, Kerl MJ, Albrecht MH, et al. Systematic Comparison of Reduced Tube Current Protocols for High-pitch and Standard-pitch Pulmonary CT Angiography in a Large Single-center Population. Acad Radiol 2016;23:619-27.
66. Lu GM, Luo S, Meinel FG, et al. High-pitch computed tomography pulmonary angiography with iterative reconstruction at 80 kVp and 20 mL contrast agent volume. Eur Radiol 2014;24:3260-8.
67. Thieme SF, Becker CT, Hacker M, et al. Dual energy CT for the assessment of lung perfusion: Correlation to scintigraphy. Eur J Radiol 2008;68:369-74.
68. Nakazawa T, Watanabe Y, Hori Y, et al. Lung perfused blood volume images with dual-0energy computed tomography for chronic thromboembolic pulmonary hypertension: correlation to scintigraphy with single-photon emission computed tomography. J Comput Assist Tomogr 2011;35:590-5.
69. Ameli-Renani S, Rahman F, Nair A, et al. Dual-energy CT for imaging of pulmonary hypertension: Challenges and opportunities. Radiographics 2014;34:1769-90
70. Pontana F, Faivre JB, Remy-Jardin M, et al. Lung perfusion with dual-energy multidetector-row CT (MDCT): feasibility for the evaluation of acute pulmonary embolism in 117 concsecutive patients. Acad Radiol 2008;15:1494-504
71. Hoey ET, Mirsadraee S, Pepke-Zaba J, et al. Dual-energy CT angiography for assessment of regional pulmonary perfusion in patients with chronic thromboembolic pulmonary hypertension: initial experience. AJR Am J Roentgenol 2011;196:524-32.
72. Bartalena T, Oboldi D, Guidalotti PL, et al. Lung perfusion in patients with pulmonary hypertension: comparison between MDCT pulmonary angiography with MiniIP reconstructions and 99m Tc-MAA perfusion scan. Invest Radiol 2008;43:368-73.
73. Pontana F, Remy-Jardin M, Duhamel A, et al. Lung perfusion with dual-energy multi-detector row CT: can it help recognize ground glass opacities of vascular origin? Acad Radiol 2010;17:587-94.
74. Lisbona R, Kreisman H, Novales-Dias JD, et al. Perfusion lung scanning: differentiation of primary from thromboembolic pulmonary hypertension. AJR Am J Roentgenol 1985;144:27-30.
75. Okada M, Kunihiro Y, Nakashima Y, et al. Added value of lung perfused blood volume images using dual-energy CT for assessment of acute pulmonary embolism. Eur J Radiol 2015;84:172-7.
76. Ameli-Renani S, Ramsay L, Bacon J. Dual-energy computed tomography in the assessment of vascular and parenchymal enhancement in suspected pulmonary hypertension. J Thorac Imaging 2014;29:98-106.
77. Meinel FG, Graef A, Thierfelder KM, et al. Automated quantification of pulmonary perfused blood volume by dual-energy CTPA in chronic thromboembolic pulmonary hypertension. Rofo 2014;186:151-6.
78. Hong YJ, Kim YY, Choe KO, et al. Different perfusion patterns between acute and chronic pulmonary thromboembolism: evaluation with two-phase dual-energy perfusion CT. AJR Am J Roentgenol 2013;200:812-7.
79. Frank H, Globits S, Glogar D, et al. Detection and quantification of pulmonary artery hypertension with MR imaging: results in 23 patients. AJR Am J Roentgenol 1993;161:27-31.
80. Swift AJ, Rajaram S, Marshall H, et al. Black blood MRI has diagnostic and prognostic value in the assessment of patients with pulmonary hypertension. Eur Radiol 2012;22:695-702.
81. Sanz J, Kuschnir P, Rius T, et al. Pulmonary arterial hypertension: noninvasive detection with phase-contrast MR imaging. Radiology 2007;243:70-9.
82. Reiter G, Reiter U, Kovacs G, et al. Blood flow vortices

along the main pulmonary artery measured with MR imaging for diagnosis of pulmonary hypertension. Radiology 2015;275:71-9.
83. Abd El Rahman MY, Hui W, Dsebissowa F, et al. Quantitative analysis of paradoxical interventricular septal motion following corrective surgery of tetralogy of fallot. Pediatr Cardiol 2005;26:379-84.
84. Brady D, Lavelle LP, McEvoy SH, et al. Assessing fibrosis in pulmonary sarcoidosis: late-enhanced MRI compared to anatomic HRCT imaging. QJM 2016;109:257-64.
85. Rajaram S, Swift AJ, Telfer A, et al. 3D contrast-enhanced lung perfusion MRI is an effective screening tool for chronic thromboembolic pulmonary hypertension: results from the ASPIRE Registry. Thorax 2013;68:677-8.
86. Arai TJ, Prisk GK, Holverda S, et al. Magnetic Resonance imaging quantification of pulmonary perfusion using calibrated arterial spin labeling. J Vis Exp 2011. doi: 10.3791/2712.
87. Lederlin M, Bauman G, Eichinger M, et al. Functional MRI using Fourier Decomposition of lung signal: reproducibility of ventilation and perfusion weighted imaging in healthy volunteers. Eur J Radiol 2013;82:1015-22.
88. Alfakih K, Plein S, Bloomer T, et al. Comparison of right ventricular volume measurements between axial and short axis orientation using steady-state free precession magnetic resonance imaging. J Magn Reson Imaging 2003;18:25-32.
89. James SH, Wald R, Wintersperger BJ, et al. Accuracy of right and left ventricular functional assessment by short-axis vs axial cine steady-state free-precession magnetic resonance imaging: intrapatient correlation with main pulmonary artery and ascending aorta phase-contrast flow measurements. Can Assoc Radiol J 2013;64:213-9.
90. Kawel-Boehm N, Maceira A, Valsangiacomo-Buechel ER, et al. Normal values for cardiovascular magnetic resonance in adults and children. J Cardiovasc Magn Reson 2015;17:29.
91. Schulz-Menger J, Bluemke DA, Bremerich J, et al. Standardized image interpretation and post processing in cardiovascular magnetic resonance: Society for Cardiovascular Magnetic Resonance (SCMR) board of trustees task force on standardized post processing. J Cardiovasc Magn Reson 2013;15:35.
92. de Siqueira ME, Pozo E, Fernandes VR, et al. Characterization and clinical significance of right ventricular mechanics in pulmonary hypertension evaluated with cardiovascular magnetic resonance feature tracking. J Cardiovasc Magn Reson 2016;18:39
93. Raymond RJ, Hinderliter AL, Willis PW, et al. Echocardiographic predictors of adverse outcomes in primary pulmonary hypertension. J Am Coll Cardiol 2002;39:1214-9.
94. Swift AJ, Wild JM, Nagle SK, et al. Quantitative magnetic resonance imaging of pulmonary hypertension: A practical approach to the current state of the art. J Thorac Imaging 2014;29:68-79.
95. Dellegrottaglie S, Sanz J, Poon M, et al. Pulmonary hypertension: accuracy of detection with left ventricular septal-to-free wall curvature ratio measured at cardiac MR. Radiology 2007;243:63-9.
96. Swift AJ, Rajaram S, Hurdman J, et al. Noninvasive estimation of PA pressure, flow and resistance with CMR imaging: derivation and validation study from ASPIRE study. JACC Cardiovasc Imaging 2013;6:1036-47.
97. Blyth KG, Groenning BA, Martin TN, et al. Contrast enhanced-cardiovascular magnetic resonance imaging in patients with pulmonary hypertension. Eur Heart J 2005;26:1993-9.
98. Shehata ML, Lossnitzer D, Skrok J, et al. Myocardial delayed enhancement in pulmonary hypertension: pulmonary hemodynamics, right ventricular function and remodeling. AJR Am J Roentgenol 2011;196:87-94.
99. Jardim C, Rochitte CE, Humbert M, et al. pulmonary artery distensibility in pulmonary arterial hypertension: an MRI pilot study. Eur Respir J 2007;29:476-81.
100. Kurzyna M, Dabrowski M, Blelecki D, et al. Atrial septostomy in treatment of end-stage right heart failure in patients with pulmonary hypertension. Chest 2007;131:977-83.
101. Berman M, Gopalan D, Sharples L, et al. Right ventricular reverse remodeling after pulmonary endarterectomy: magnetic resonance imaging and clinical and right heart catheterization assessment. Pulm Circ 2014;4:36-44.
102. Barst RJ, McGoon M, Torbicki A, et al. Diagnosis and differential assessment of pulmonary arterial hypertension. J Am Coll Cardiol 2004;43:40S-7S.
103. Trow TK, McArdle JR. Diagnosis of pulmonary arterial hypertension. Clin Chest Med 2007;28:59-73-viii.
104. Bradlow WM, Gibbs JS, Mohiaddin RH. Cardiovascular magnetic resonance in pulmonary hypertension. J Cardiovasc Magn Reson 2012;14:6.

Cite this article as: Goerne H, Batra K, Rajiah P. Imaging of pulmonary hypertension: an update. Cardiovasc Diagn Ther 2018;8(3):279-296. doi: 10.21037/cdt.2018.01.10

